



science.sciencemag.org/cgi/content/full/science.abe6959/DC1

Supplementary Material for **Model-informed COVID-19 vaccine prioritization strategies by age and serostatus**

Kate M. Bubar*, Kyle Reinholt, Stephen M. Kissler, Marc Lipsitch, Sarah Cobey,
Yonatan H. Grad, Daniel B. Larremore*

*Corresponding author. E-mail: kate.bubar@colorado.edu (K.M.B.);
daniel.larremore@colorado.edu (D.B.L.)

Published 21 January 2021 as *Science* First Release
DOI: [10.1126/science.abe6959](https://doi.org/10.1126/science.abe6959)

This PDF file includes:

Materials and Methods
Supplementary Text
Figs. S1 to S15
Tables S1 and S2
References

Other Supplementary Material for this manuscript includes the following:
(available at science.sciencemag.org/content/science.abe6959/DC1)

MDAR Reproducibility Checklist

Materials and Methods

Susceptible Exposed Infectious Recovered (SEIR) Model Overview

We used a continuous-time ordinary differential equations (ODE) compartmental model stratified by age. Across all model variations and analyses, we simulated 365 days of dynamics, corresponding to the first-year phase of vaccine prioritization. All individuals were assumed to be initially susceptible, unless they had been effectively vaccinated or had naturally acquired immunity, which was considered to be protective in this model. Susceptible people (S) transition to the exposed state (E) after contact with an infectious individual. After a latent period, exposed individuals become infectious (I). After an infectious period, individuals move to a recovered state (R) or die. We assume that recovered individuals are no longer infectious and are immune to reinfection over the duration of simulations (up to 365 days). The duration of time spent in compartments E and I , in expectation, are specified in Table S1. Model equations were solved using *lsoda* ODE solver from the package *deSolve*, R version 3.6.0 (55). Fig. S1 shows model schematic diagrams for the variations of the SEIR model considered in this manuscript.

The force of infection, λ_i for a susceptible individual in age group i is

$$\lambda_i = u_i \sum_j c_{ij} \frac{I_j + I_{vj} + I_{xj}}{N_j - \Omega_j},$$

where u_i is the probability of a successful transmission given contact with an infectious individual and c_{ij} is the number of age- j individuals that an age- i individual contacts per day. The term $(I_j + I_{vj} + I_{xj})/(N_j - \Omega_j)$ is the probability that a random age- j individual is infectious, where I_j is the number of individuals who are unvaccinated and infectious, I_{vj} is the number of individuals who are vaccinated yet infectious, I_{xj} is the number of individuals who are ineligible for vaccination (e.g. due to hesitancy or due to a positive serological test) and infectious, N_j is the total number of individuals in group j and Ω_j is the number of individuals from group j who have died. To calculate the basic reproductive number, R_0 , we define the next-generation matrix as

$$M = D_u C D_{d_I},$$

where D_u is a diagonal matrix with diagonal entries u_i , C is the country-specific contact matrix, and D_{d_I} is a diagonal matrix with diagonal entries d_I , the infectious period. R_0 is the absolute value of the dominant eigenvalue of M . Age-stratified susceptibility values were drawn from literature estimates (13). Table S1 details all parameters used in this manuscript and their sources.

Incorporation of Vaccine Hesitancy

To incorporate vaccine hesitancy, we limited vaccine uptake such that at most 70% of any age group was eligible to be vaccinated (24). To implement this restriction, 30% of each compartment for each age group was initialized as ineligible for vaccination. These individuals were tracked using compartments S_x , E_x , I_x , and R_x (Fig. S1). Initial conditions, inclusive of 30% vaccine hesitancy, are listed in Table S2.

Incorporation of Vaccination, Vaccine Rollout, and Vaccine Efficacy

In the simplest version of the model, the vaccine is assumed to be transmission- and infection- blocking, and to work with variable efficacy. We considered two classes of scenarios. In the first class of scenarios, vaccinations are given in advance of model dynamics, which we call pre-transmission vaccination. In the second class of scenarios, vaccinations are rolled out at the same time as the model dynamics, which we call continuous rollout vaccination.

In continuous rollout scenarios (Scenarios 1 and 2), vaccine rollout was parameterized by the percentage of the total population that was vaccinated in each day of simulation, with values ranging from 0.05% to 1% of total population (see Fig. S6). Scenarios 1 and 2 of the Main Text consider rollout speeds of 0.2% per day. The prescribed number of individuals received the effects of vaccination in simulations prior to the start of each day, such that disease dynamics proceeded in continuous time while vaccine rollout was computed in discrete steps. We did not include an explicit delay between vaccination and protection, and therefore our approach may be thought of as either a model for a vaccine with immediate protective effects, or as a model in which the time of protection is explicitly modeled and injections are thus implicitly assumed to precede said protection. In continuous rollout scenarios, the model was seeded with 0.25% of individuals in each age group exposed and 0.25% of individuals in each age group infectious.

In pre-transmission vaccination scenarios (Scenario 3 and 4), all the available vaccines were distributed at the initial time step, prior to the epidemic. To incorporate vaccinations, we initialized the model by dividing the total population of each age group between the susceptible compartment (S) and vaccinated compartment (V or S_v), according to the vaccine prioritization strategy and number of vaccines available. In pre-transmission vaccination scenarios, the model was seeded with one infectious person in I and one infectious person in I_x in each age group. Scenarios 3 and 4 of the Supplementary Text use pre-transmission rollout.

We considered two ways to implement vaccine efficacy (ve): as an all-or-nothing vaccine, where the vaccine provides perfect protection to a fraction ve of individuals who receive it, or as a leaky vaccine, where all vaccinated individuals have reduced probability ve of infection after vaccination (see Supplementary Text). We ran simulations with both types of vaccine efficacy; Figures in the Main Text show results only for all-or-nothing vaccines.

To incorporate age-dependent vaccine efficacy, we parameterized the relationship between age and vaccine efficacy via an age-efficacy curve with (i) a baseline efficacy, an age at which efficacy begins to decrease (hinge age), and a minimum vaccine efficacy ve_m for adults 80+ (Fig. 3A). We assumed that ve is equal to the baseline value for all ages younger than the hinge age, then decreases stepwise in equal increments for each decade to the specified minimum ve_m for the 80+ age group. To determine whether there exists a ve_m such that the mortality-minimizing strategy switches from directly vaccinating adults 60+ to an alternative strategy, we used the bisection method (56).

Incorporation of Existing Seroprevalence

To incorporate existing seroprevalence estimates and compare areas with differing naturally-acquired immunity, we used data and seroprevalence estimates from Connecticut [low seroprevalence; (31)]

and New York City [moderate seroprevalence; (30)]. To model high seroprevalence, we simulated an unmitigated epidemic with $R_0 = 2.6$ until 40% cumulative incidence was reached. Seroprevalence was implemented by moving the proportion of seropositive individuals from each age group into the recovered compartment prior to forward simulations that incorporated vaccination.

The model’s implementation of vaccination depended on whether the vaccine was rolled out during on-going transmission or prior to transmission. For pre-transmission vaccination without consideration of serostatus, v_i doses were given to each population group i , a fraction θ_i of whom were already recovered. Thus, the total number of individuals eligible for vaccination were $S + R$, assuming currently infected individuals do not seek vaccination. In scenarios where vaccination was targeted only at seronegative individuals, simulations were conducted with sensitivity 70% and specificity 99%, incorporating the performance of a hypothetical Euroimmun IgG test (35) and a 25% reduction in sensitivity due to seroreversion (32). Details of continuous vaccine rollout with dose redirection using an imperfect serological test can be found in Supplementary Text.

Calibration to achieve target R_0

Models were calibrated to achieve the target R_0 by multiplying the next-generation matrix by a constant to achieve the desired dominant eigenvalue, i.e. R_0 . Because the constant factors out of the next-generation matrix equation, this may be mathematically interpreted as scaling up or down either the contact rates C or susceptibilities u . All model calibration was performed prior to the inclusion of vaccination, meaning that the reproductive number R in the first days of a simulation may differ from R_0 depending on the scenario considered. Values of R_0 studied ranged from 1.1 to 2.6. When incorporating seroprevalence, calibration was performed after the inclusion of seroprevalence.

Measurement of outcomes: infections, deaths, and years of life lost

We ran simulations for 365 days from the date of the first vaccination to focus on the early prioritization phase of the COVID-19 vaccination programs. To compare the impact of different vaccination prioritization strategies, we calculated the cumulative number of infections and deaths. Infected individuals either move to the recovered or dead compartment, according to the age-dependent IFR (19) (see Fig. S1). The cumulative number of new infections since the onset of vaccine rollout is the total number of recovered and dead at the end of the simulation minus the initial number of seropositive individuals, $\sum_i R_i + R_{x,i} + R_{v,i} + \Omega_i - \theta_i N_i$. The total number of estimated deaths was the number of people in the dead compartment at the end of the simulation. To calculate years of life lost (YLL) due to a death at a particular age, we multiplied standard life expectancy (SLE) by the number of deaths per age bin. We used the country-specific SLE estimates from the WHO Global Health Observatory (57), aggregated into age bins by decade using $YLL_i = \frac{1}{10} \sum_j YLL_j$ where j are the ages corresponding to decadal age bin i .

Contact Matrices and Demographics

Country-specific contact matrices include four types of contact: home, work, school, and other (22). In all simulations, we used total contact matrices, equivalent to the sums of the four contact types. Age demographics in all simulations were taken from the UN World Population Prospects 2019 for each

country (23). Age bins in each case were originally provided in 5-year increments, which were then combined into 10-year increments by addition. For instance, the number of individuals between 20 and 29 was the sum of individuals 20-24 and 25-29. The number of individuals 80 years and older was calculated as the sum of all age bins greater than 80.

We made two adaptations to existing contact matrices (22). First, we combined their five year age bins into ten year bins. Each entry x_{ij} in the original matrices corresponds to the number of individuals of age-group j that a person in age group i typically comes into contact with. Thus, for a country with population fraction d_i in age group i , the combined contact matrix entries are given by

$$c_{ij} = \frac{d_{2i}(x_{2i,2j} + x_{2i,2j+1}) + d_{2i+1}(x_{2i+1,2j} + x_{2i+1,2j+1})}{d_{2i} + d_{2i+1}}.$$

Second, we extrapolated matrices to include individuals 80+. To extrapolate, we copied the contact rates from 70-79 y to our new row and column for 80+, along the diagonal. Then we filled in the end of our new row and column with the 70-79 y contact rates with 0-9 y, assuming interactions with 0-9 y are similar for people 70+. Lastly, to account for increased housing in long term living facilities for 80+ y, we decreased their contacts for 0-60 y by 10% and added it to the 70 and 80 y contacts. Thus, 80+ year-olds have the same total number of contacts as 70-79 year-olds, but relatively fewer among 0-69-year-olds and proportionally more among 70+ year-olds.

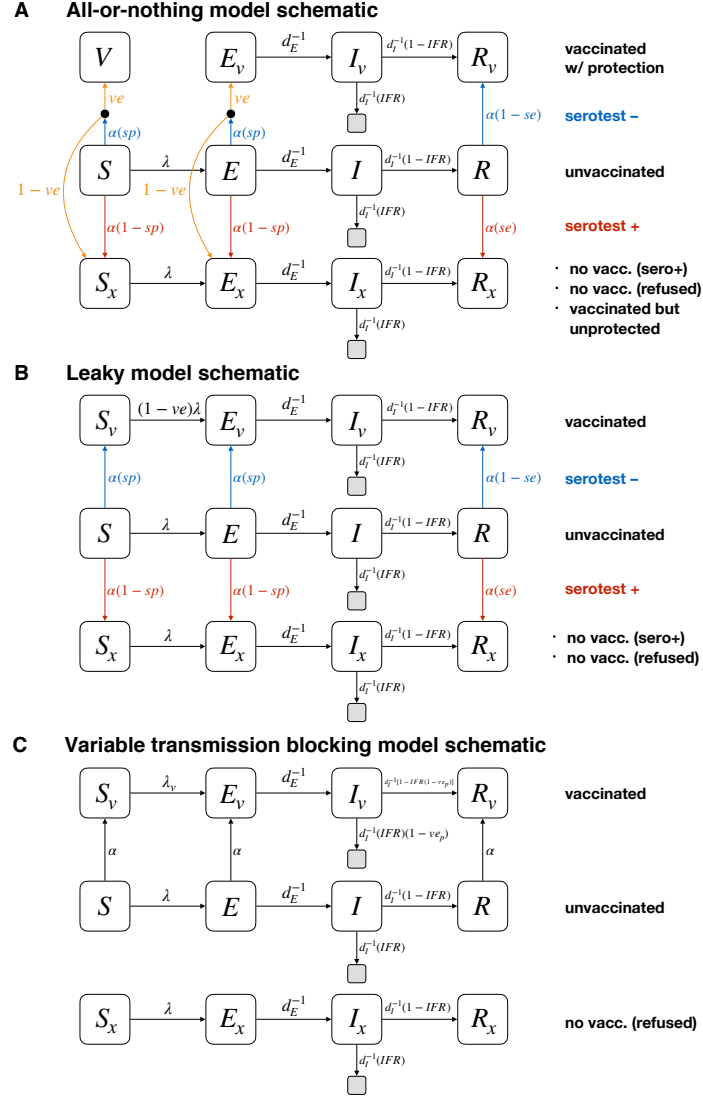


Figure S1: Schematics for vaccine modeling framework. Diagrams show compartmental models and transition rates for the (A) all-or-nothing, (B) leaky, and (C) variable transmission-blocking vaccine models used in this manuscript. S , E , I , and R represent susceptible, exposed, infectious, and recovered compartments; V represents a perfectly protected and vaccinated compartment; subscripts of v and x denote those who have been vaccinated with protection (v), and those who will either not be vaccinated (vaccine refusal or positive serotest) or have been vaccinated but without protection (x). Grey unlabeled compartments represent death. The incorporation of a point-of-care serological test can be included by using known sensitivity se and specificity sp , or can be excluded by setting $se = 0$ and $sp = 1$ (a convenient mathematical representation of the no-test scenario is simply a test that always returns a negative result). Vaccine rollout count α is given by $\alpha = n_{\text{vax}} / [(S + E)sp + R(1 - se)]$ where n_{vax} is the total number of vaccines to be rolled out in a particular day. All compartments are stratified by age, in the text, with index i . See text for details and initial conditions.

Supplementary Text

SEIR Model Modifications

The flexible age-stratified SEIR model framework allowed us to model (i) leaky or all-or-nothing vaccine efficacy, (ii) variable rollout speeds, (iii) point-of-care reprioritization of vaccines using an imperfect serological test, and (iv) the possibility of only partial transmission blocking effects, through straightforward modifications. The framework is shown in Fig. S1, and explicitly tracks individuals who were vaccinated and protected, vaccinated but not protected (all-or-nothing model only), considered for vaccination but did not receive a dose due to a positive serological test, and those who were not vaccinated or considered for vaccination. These four modes of operation are described in the subsections below.

Implementing vaccine efficacy: leaky vs all-or-nothing

A vaccine with imperfect efficacy can be modeled as either a “leaky” vaccine, where all vaccinated individuals are *ve* protected against infection (Fig. S1A), or an “all-or-nothing” vaccine, where a fraction *ve* of vaccinated individuals are perfectly protected while the remaining $1 - ve$ individuals gain no protection (Fig. S1B). We considered both model implementations of vaccine efficacy, showing results for the all-or-nothing model in the Main Text and the leaky model in Supplementary Figures, as indicated in figure captions.

Implementing variable vaccine rollout rate

We allowed vaccines to be distributed (or “rolled out”) at different rates by parameterizing the number of vaccines available in each simulated day, n_{vax} . In each simulated day, exactly n_{vax} doses are distributed, according to the prioritization strategy, prior to calculating new exposures, infections, and recoveries. As a result, pre-transmission vaccination, in which all doses are used prior to SEIR dynamics, can be implemented by setting n_{vax} equal to the total number of doses available. In all scenarios, when all doses have been used, $n_{\text{vax}} = 0$ for all timesteps thereafter.

Implementing point-of-care dose redirection with imperfect serological tests

The modeling framework depicted in Fig. S1 allows for the point-of-care reprioritization of tests by using the outcome of an imperfect serological test with sensitivity *se* and specificity *sp*. We assume that only those who test negative receive a vaccine, but that this population may consist of true negatives from the *S* or *E* compartments or false negatives from the *R* compartment. By tracking all such individuals, we prevent the model from vaccinating the same person twice. Similarly, we assume that those who test positive do not receive a vaccine at any point after testing positive. These include false positives from the *S* and *E* compartments and true positives from the *R* compartment.

The numbers of individuals who receive a vaccination each timestep, given a supply of n_{vax} to be allo-

cated in that timestep, are

$$\begin{aligned}
S \rightarrow S_v &= \frac{n_{\text{vax}}}{(S + E)sp + R(1 - se)} S(sp) \\
E \rightarrow E_v &= \frac{n_{\text{vax}}}{(S + E)sp + R(1 - se)} E(sp) \\
R \rightarrow R_v &= \frac{n_{\text{vax}}}{(S + E)sp + R(1 - se)} R(1 - se)
\end{aligned} \tag{S1}$$

while the numbers of individuals who are tested but are excluded from vaccination are

$$\begin{aligned}
S \rightarrow S_x &= \frac{n_{\text{vax}}}{(S + E)sp + R(1 - se)} S(1 - sp) \\
E \rightarrow E_x &= \frac{n_{\text{vax}}}{(S + E)sp + R(1 - se)} E(1 - sp) \\
R \rightarrow R_x &= \frac{n_{\text{vax}}}{(S + E)sp + R(1 - se)} R(se)
\end{aligned} \tag{S2}$$

How many more susceptible individuals get vaccinated when point-of-care reprioritization is used? This can be computed *a priori* for pre-transmission rollouts in which a fraction θ_i of individuals in subpopulation i are truly seropositive and thus treated as recovered. If we further assume no ongoing transmission, then $S = (1 - \theta_i)N(1 - vh)$ where vh is the fraction of each age group that is vaccine hesitant, and the number of susceptible individuals vaccinated is

$$\frac{n_{\text{vax},i}}{(1 - \theta_i)sp + \theta_i(1 - se)} (1 - \theta_i)sp,$$

while the number of susceptible individuals vaccinated without point-of-care serology is

$$n_{\text{vax},i}(1 - \theta_i).$$

We note that vaccination without a serotest is equivalent to setting $se = 0$ and $sp = 1$, i.e. considering a “test” that always returns a negative result. The relative increase in the number of individuals vaccinated is thus

$$\text{relative increase in susceptibles vaccinated} = \frac{sp}{(1 - \theta_i)sp + \theta_i(1 - se)} - 1. \tag{S3}$$

Recent work suggests that seroprevalence decreases over time due to seroreversion (32). As a consequence, Eq. S3 and the calculations used to derive it must be interpreted with care. If θ_i represents the current seroprevalence, Eq. (S3) may be used with the published sensitivity and specificity of a serological test (e.g. 99% specificity and 96% sensitivity for the Euroimmun IgG (35)). However, if θ_i represents a past measurement of seroprevalence or an estimate of cumulative incidence, then the sensitivity of a test to identify individuals with past exposure will be diminished, with estimates suggesting seroreversion of 27% of individuals over 3 months (32). To more conservatively estimate the impact of using serology for dose redirection, a test with 70% sensitivity and 99% specificity in a population with a past measurement of 25% seropositivity would lead to a 21.1% increase in susceptibles vaccinated. When vaccine rollout is not pre-transmission, and instead continues alongside transmission, *a priori* calculations of this type are not possible.

Implementing vaccines with imperfect transmission blocking

We considered a vaccine that prevents severe manifestations of COVID-19 infection, including death, with 90% efficacy, but imperfectly blocks transmission of SARS-CoV-2 (Fig. S1C). To model such a vaccine, we modify the leaky vaccine model by introducing three different mechanisms for vaccine efficacy: ve_S is the efficacy of the vaccine to decrease susceptibility; ve_I is the efficacy of the vaccine to decrease infectiousness; and ve_P is the efficacy of the vaccine to decrease the likelihood that the infection progresses to severe disease and death.

In this model, the infectiousness of vaccinated individuals is decreased by a factor of $1 - ve_I$. Second, the susceptibility of vaccinated individuals is decreased by a factor of $1 - ve_S$. This results in a force of infection for unvaccinated individuals of

$$\lambda_i = u_i \sum_j c_{ij} \frac{I_j + (1 - ve_I)I_j^V}{N_j - \Omega_j}$$

and a force of infection for vaccinated individuals of

$$\lambda_{i,V} = (1 - ve_S)\lambda_i .$$

These values of λ_i replace previous values of λ_i for $S \rightarrow I$ transitions, and values of $\lambda_{i,V}$ replace values of $(1 - ve)\lambda_i$ for $S_V \rightarrow I_V$ transitions (see Fig. S1). Finally, the fatality rate, conditioned on infection, is multiplied by a factor of $1 - ve_P$.

The impact of this variable-transmission blocking model on minimizing incidence and mortality are shown in Supplementary Fig. S10 for $ve_S = 0$, $ve_P = 90\%$ and $ve_I = 0 - 100\%$. Note that when $ve_S = ve_I = 0$, there are no indirect effects of vaccination. Finally, we note that when considering a leaky vaccine with different effects on infection, transmission, and progression, the parameterization could be accomplished in any of several ways. Ours makes the choice for simplicity to consider the vaccine's entire effect to be on infectiousness and progression.

Results for Pre-Transmission Vaccine Rollout

The governments and residents of New Zealand, Taiwan, and South Korea, among others, have been dramatically more successful at mitigating the spread of SARS-CoV-2 than the rest of the world. As a result, widespread vaccination is likely to occur prior to the reopening of external borders and the relaxation of restrictions and testing of incoming travellers. To better model these particular scenarios, we conducted additional analyses using pre-pandemic contact matrices but implemented vaccination prior to the start of model dynamics. Here, we review our findings for such pre-transmission vaccination with $R_0 = 1.5$ (Scenario 3) and $R_0 = 2.6$ (Scenario 4).

Of the five strategies, direct vaccination of adults over 60 years (60+) nearly always reduced mortality and YLL more than the alternative strategies when transmission was high, across vaccine efficacies and supplies ($R_0 = 2.6$; Scenario 4, Fig. S5). Exceptions occurred only vaccine efficacy was 80% or higher and supply was sufficient to cover over 45% of the population (Fig. S5). However, when transmission was lower ($R_0 = 1.5$; Scenario 3), prioritizing adults 20-49 most reduced mortality in a similarly broad range of vaccine efficacies and supplies (Fig. S5).

Across countries, a general pattern emerged in which prioritization of adults 60+ was more often the mortality-minimizing strategy when transmission was higher and adults 20-49 when transmission was lower (Scenario 4 vs Scenario 3). However, for many vaccine supply levels and 90% vaccine efficacy, the prioritization of adults 20+ was also optimal (Fig. S9).

Across all scenarios, vaccine supplies, efficacies, and values of R_0 , the prioritization of adults 20-49 most reduced cumulative incidence in pre-transmission vaccination, with two exceptions. First, for high transmission ($R_0 = 2.6$; Scenario 4), vaccination of those under 20 was most effective when efficacy was under 60%, a result restricted to the leaky vaccine model (Fig. S7). Second, for high transmission ($R_0 = 2.6$; Scenario 4), vaccination of those under 20 was most effective when transmission-blocking efficacy was imperfect and vaccine supplies were low or moderate (Fig. S10).

Direct comparison of Scenario 2 ($R_0 = 1.5$, rollout 0.2% per day) and Scenario 3 ($R_0 = 1.5$, pre-transmission vaccination) shows that the ability to vaccinate prior to transmission markedly changes optimal strategies. These results were unaffected by modeling the vaccine as all-or-nothing (Fig. S5) or leaky (Fig. S7), except that for vaccine efficacy below 60% and high transmission (Scenario 4), prioritization of those under 20 most reduced transmission.

In general, pre-transmission vaccination markedly reduced both mortality and transmission, and expanded the vaccine supply and efficacy combinations for which prioritizing adults 20-49 most reduced mortality and YLL across all investigated values of R_0 (Fig. S8), and across countries (Fig. S9), relative to mid-epidemic vaccine rollout.

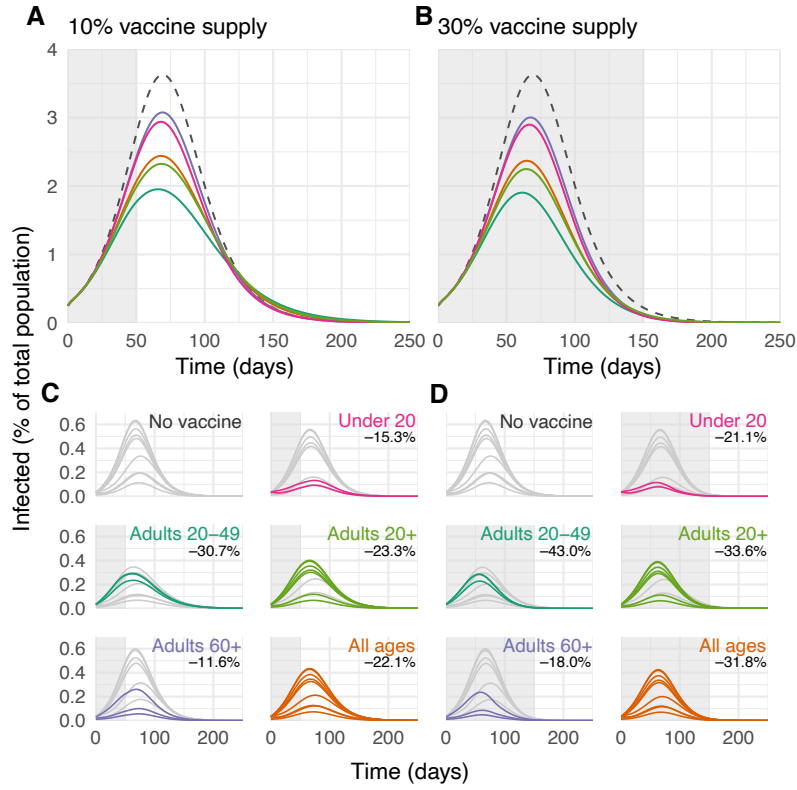


Figure S2: Example infection curves under varying vaccine supply and prioritization strategy. (A, B) The percentage of the total population infected over time is shown during simulations with no vaccines (grey dashed lines) and for five different prioritization strategies, with 10% (A) and 30% (B) vaccine supply. (C, D) The percentage of the total population infected over time, stratified into the decadal age groups used in simulations, are shown for both prioritized age groups (colored lines) and unvaccinated age groups (grey lines), with 10% (C) and 30% (D) vaccine supply. Annotations indicate the age groups targeted by each strategy and record the total reductions in infections after 365 simulated days. Shown: contact patterns and demographics of the United States (22,23); all-or-nothing and transmission blocking vaccine, $R_0 = 1.5$, $ve = 90\%$, rollout speed 0.2% of the population per day. See Figs. S3 and S4 for cumulative incidence and mortality curves.

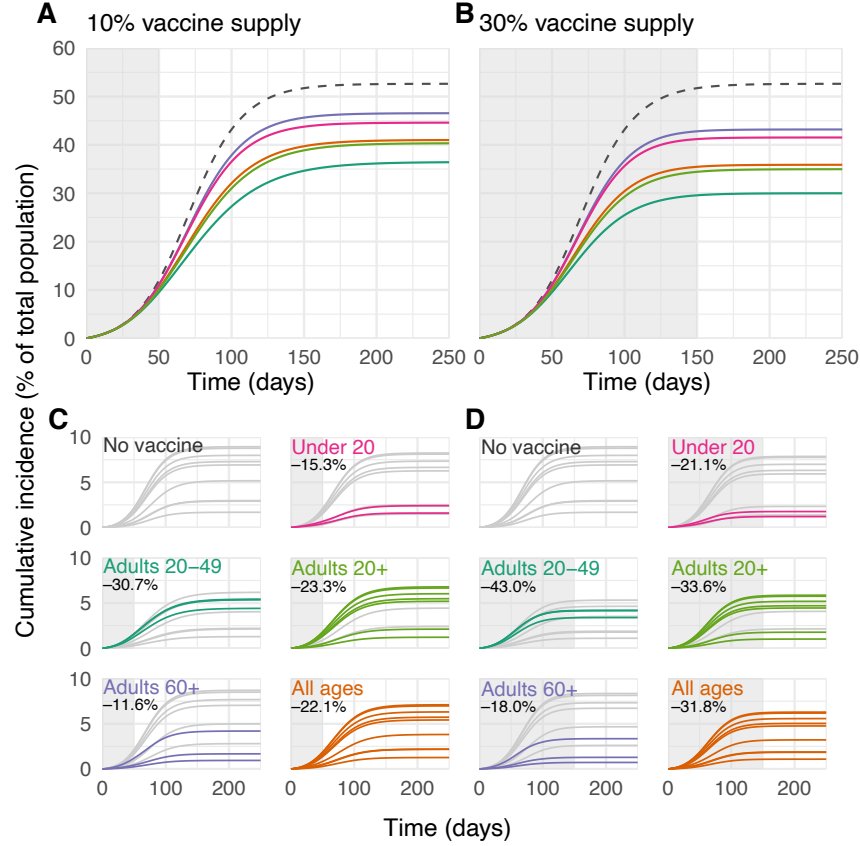


Figure S3: Example cumulative incidence curves under varying vaccine supply and prioritization strategy. (A, B) The percentage of the total number of infections over time is shown during simulations with no vaccines (grey dashed lines) and for five different prioritization strategies, with 10% (A) and 30% (B) vaccine supply. (C, D) The percentage of the total number of infections over time, stratified into the decadal age groups used in simulations, are shown for both prioritized age groups (colored lines) and unvaccinated age groups (grey lines), with 10% (C) and 30% (D) vaccine supply. Annotations indicate the age groups targeted by each strategy and record the total reductions in infections after 365 simulated days. Shown: contact patterns and demographics of the United States (22, 23); all-or-nothing and transmission blocking vaccine, $R_0 = 1.5$, vaccine efficacy=90%, rollout speed 0.2% of the population per day. See Figs. S2 and S4 for infections and cumulative mortality curves.

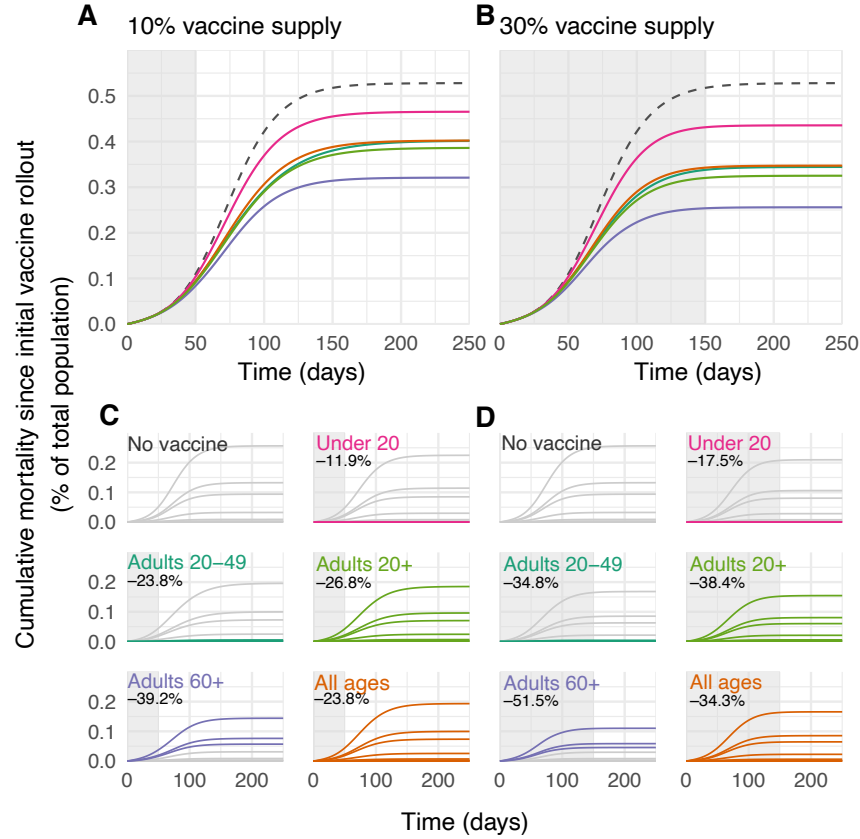


Figure S4: Example cumulative mortality curves under varying vaccine supply and prioritization strategy. (A, B) The cumulative mortality as a percentage of the total population is shown during simulations with no vaccines (grey dashed lines) and for five different prioritization strategies, with 10% (A) and 30% (B) vaccine supply. (C, D) The cumulative mortality as a percentage of the total population, stratified into the decadal age groups used in simulations, are shown for both prioritized age groups (colored lines) and unvaccinated age groups (grey lines), with 10% (C) and 30% (D) vaccine supply. Annotations indicate the age groups targeted by each strategy and record the total reductions in infections after 365 simulated days. Shown: contact patterns and demographics of the United States (22, 23); all-or-nothing and transmission blocking vaccine, $R_0 = 1.5$, vaccine efficacy=90%, rollout speed 0.2% of the population per day. See Fig. S2 and S3 for infections and cumulative incidence curves.

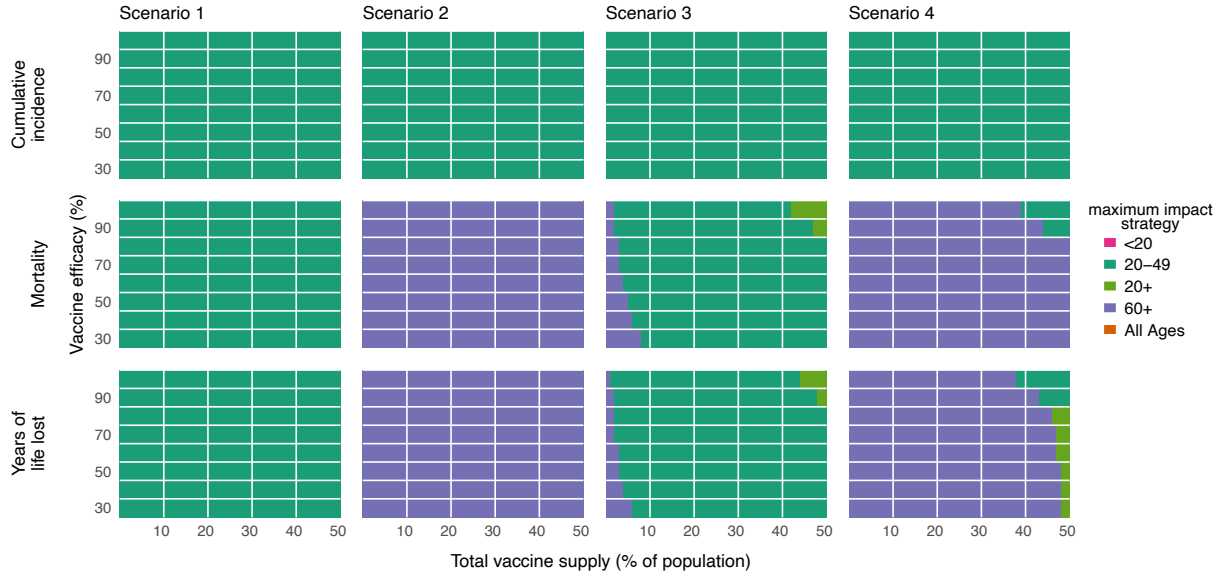


Figure S5: Impact of vaccine efficacy on maximum impact strategies (all-or-nothing vaccine). Heatmaps show the prioritization strategies resulting in maximum reduction of infections (top row), mortality (middle row), and years of life lost (bottom row) across Scenario 1 (0.2% rollout/day, $R_0 = 1.15$; left column), Scenario 2 (0.2% rollout/day, $R_0 = 1.5$; left-middle column), Scenario 3 (pre-transmission vaccination, $R_0 = 1.5$; right-middle column), and Scenario 4 (pre-transmission vaccination, $R_0 = 2.6$; right column). Each heatmap shows results from simulations varying vaccine supply and vaccine efficacy as indicated. Shown: contact patterns and demographics of the United States (22, 23); all-or nothing and transmission blocking vaccine. See Fig. S7 for leaky vaccine results.

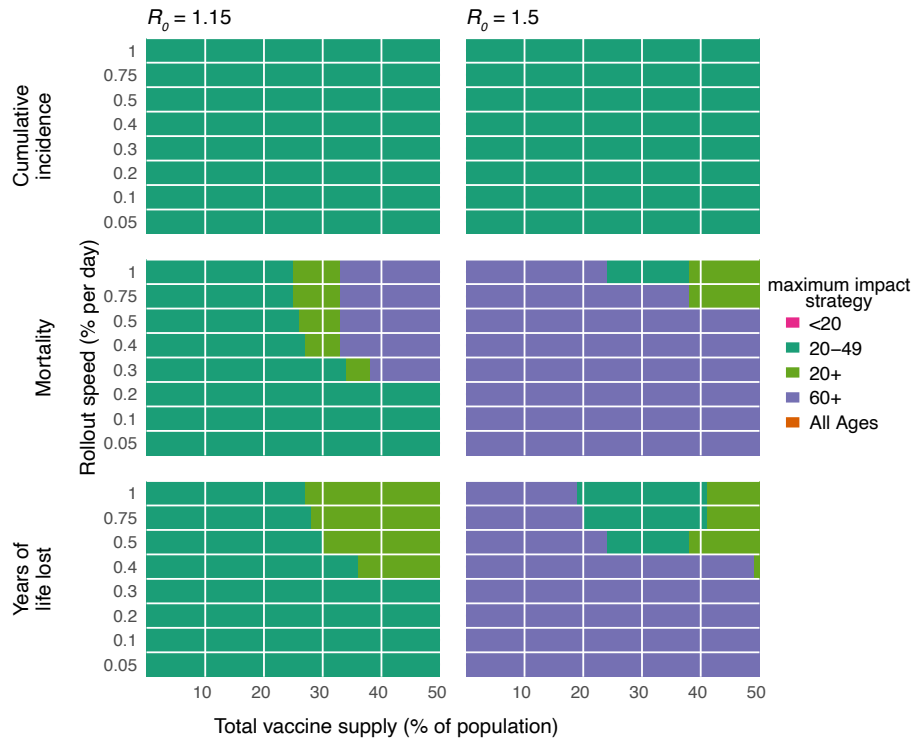


Figure S6: **Impact of rollout speed on maximum impact strategies.** Heatmaps show the prioritization strategies resulting in maximum reduction of infections (top row), mortality (middle row), and years of life lost (bottom row) for $R_0 = 1.15$ (left column) or $R_0 = 1.5$ (right column). Each heatmap shows results from simulations varying vaccine supply and the rollout speed of the vaccine, measured in the percentage of the total population vaccinated per day. Shown: contact patterns and demographics of the United States (22, 23); all-or nothing and transmission blocking vaccine, with vaccine efficacy = 90%.

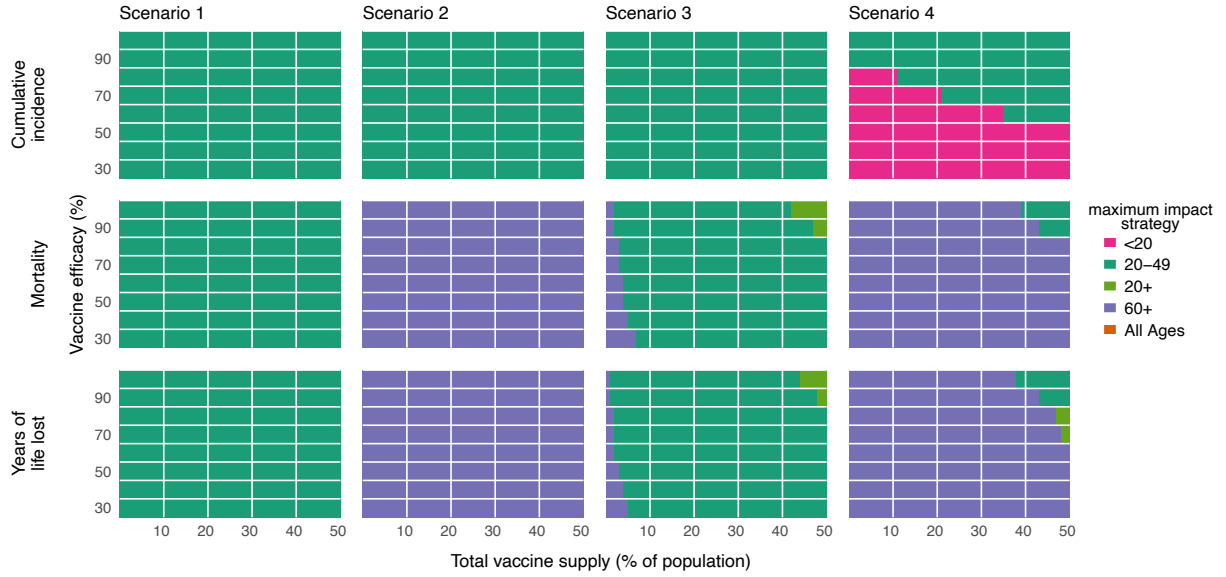


Figure S7: **Impact of vaccine efficacy on maximum impact strategies (leaky vaccine).** Heatmaps show the prioritization strategies resulting in maximum reduction of infections (top row), mortality (middle row), and years of life lost (bottom row) across Scenario 1 (0.2% rollout/day, $R_0 = 1.15$; left column), Scenario 2 (0.2% rollout/day, $R_0 = 1.5$; left-middle column), Scenario 3 (pre-transmission vaccination, $R_0 = 1.5$; right-middle column), and Scenario 4 (pre-transmission vaccination, $R_0 = 2.6$; right column). Each heatmap shows results from simulations varying vaccine supply and vaccine efficacy as indicated. Shown: contact patterns and demographics of the United States (22, 23); leaky and transmission blocking vaccine. See Fig. S5 for all-or-nothing vaccine results.

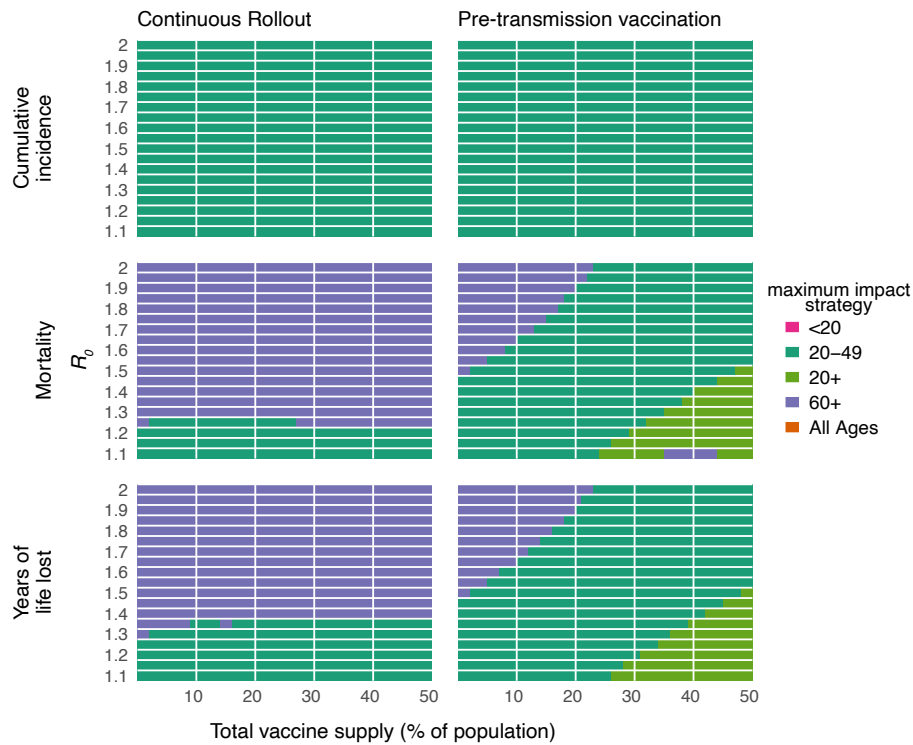


Figure S8: **Impact of reproductive number R_0 on maximum impact strategies.** Heatmaps show the prioritization strategies resulting in maximum reduction of infections (top row), mortality (middle row), and years of life lost (bottom row) for a continuous rollout scenario (0.2% rollout/day; left column) or a pre-transmission rollout scenario (all doses administered prior to simulations; right column). Each heatmap shows results from simulations varying vaccine supply and the basic reproductive number R_0 . Shown: contact patterns and demographics of the United States (22, 23); all-or nothing and transmission blocking vaccine, with vaccine efficacy=90%.

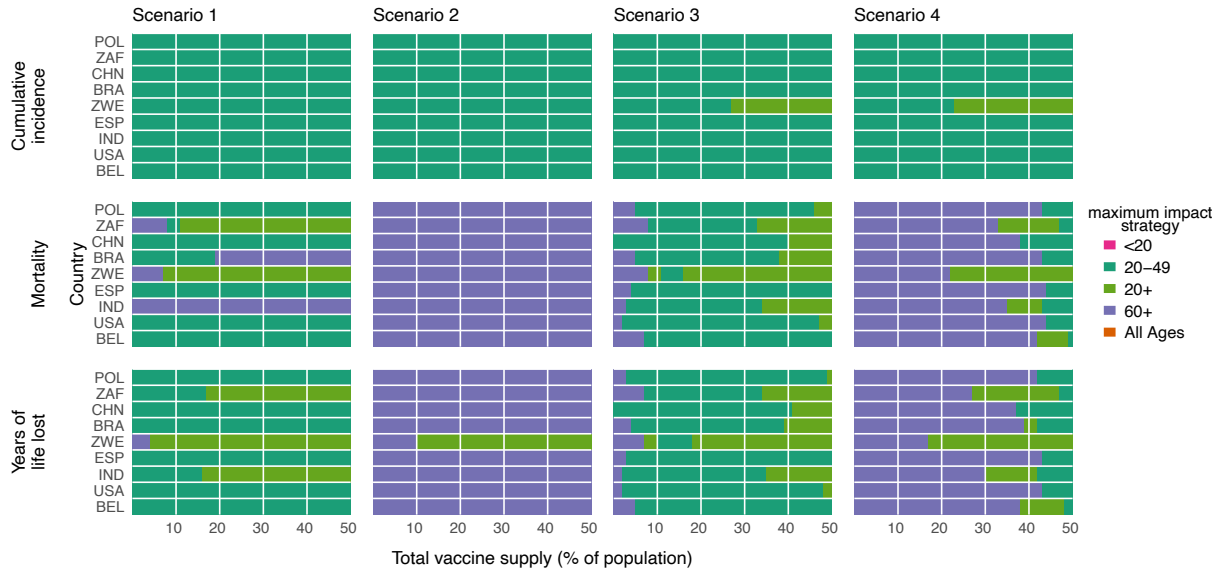


Figure S9: Impact of country demography and contact patterns on maximum impact strategies. Heatmaps show the prioritization strategies resulting in maximum reduction of infections (top row), mortality (middle row), and years of life lost (bottom row) across Scenario 1 (0.2% rollout/day, $R_0 = 1.15$; left column), Scenario 2 (0.2% rollout/day, $R_0 = 1.5$; left-middle column), and Scenario 3 (pre-transmission vaccination, $R_0 = 1.5$; right-middle column), and Scenario 4 (pre-transmission vaccination, $R_0 = 2.6$; right column). Each heatmap shows results from simulations varying vaccine supply and the country whose demographics and contact patterns were modeled (22, 23). Shown: all-or-nothing and transmission blocking vaccine, with vaccine efficacy=90%. POL, Poland; ZAF, South Africa; CHN, China; BRA, Brazil; ZWE, Zimbabwe; ESP, Spain; IND, India; USA, United States of America; BEL, Belgium.



Figure S10: **Impact of imperfect transmission-blocking effects on maximum impact strategies.** Heatmaps show the prioritization strategies resulting in maximum reduction of infections (top row), mortality (middle row), and years of life lost (bottom row) across Scenario 1 (0.2% rollout/day, $R_0 = 1.15$; left column), Scenario 2 (0.2% rollout/day, $R_0 = 1.5$; left-middle column), Scenario 3 (pre-transmission vaccination, $R_0 = 1.5$; right-middle column), and Scenario 4 (pre-transmission vaccination, $R_0 = 2.6$; right column). Each heatmap shows results from simulations varying vaccine supply and the vaccine's efficacy in blocking transmission v_{e_I} as indicated. Because the bottom row of cumulative incidence plots corresponds to a vaccine with 0% efficacy to reduce transmission, the row is grey indicated no maximum impact prioritization. Shown: contact patterns and demographics of the United States (22, 23), for a vaccine with protective efficacy from severe disease $v_{e_P} = 0.9$ and no efficacy for protection from infection $v_{e_S} = 0$. See Supplementary Text for modeling details.

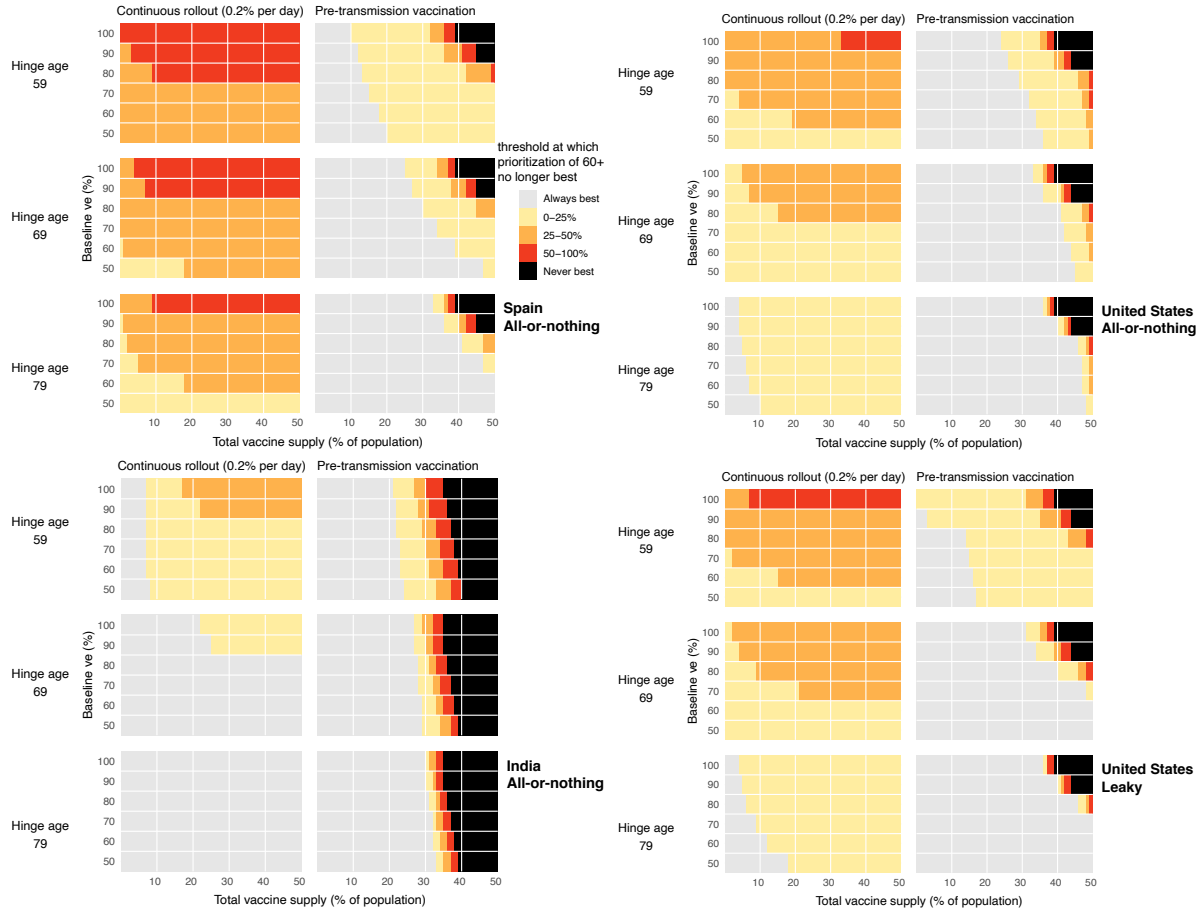


Figure S11: **Impact of age-related decreases in vaccine efficacy on vaccine prioritization.** Heatmaps show that prioritization of adults 60+ to minimize mortality remains generally robust to large decreases in vaccine efficacy among older adults. Each point shows the threshold value of vaccine efficacy among adults 80+ at which prioritizing adults 60+ is no longer the best strategy to minimize mortality, if one exists (yellow, orange, red), or indicates that none exists (grey). Parameter combinations for which mortality is never minimized by prioritization of adults 60+ are also shown (black). Panels show combinations of the age at which immunosenescence begins (hinge age), total vaccine supply, and baseline efficacy for continuous (0.2% per day, $R_0 = 1.5$) and pre-transmission rollout scenarios with $R_0 = 2.6$ for (A) Spain, (B) the United States, and (C) India, using an all-or-nothing vaccine model; (D) the United States, using a leaky vaccine model.

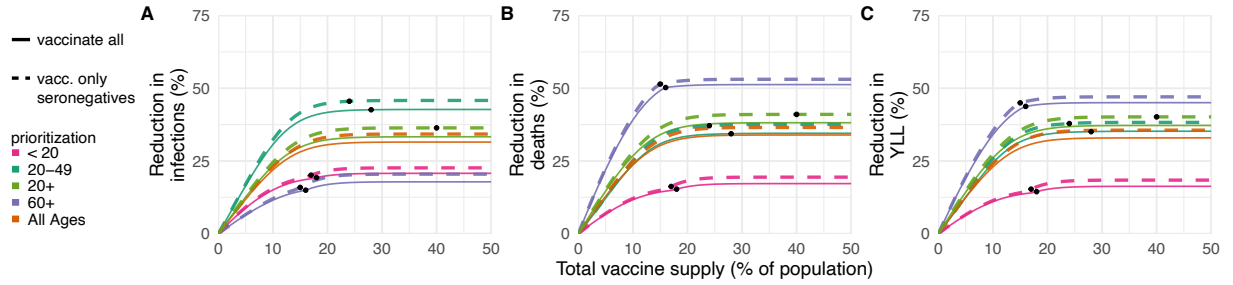


Figure S12: **Effects of existing seropositivity on the impacts of prioritization strategies (low seroprevalence).** Percent reductions in (A) infections, (B) deaths, and (C) years of life lost (YLL) for prioritization strategies when existing age-stratified seroprevalence is incorporated (July 2020 estimates for Connecticut; mean seroprevalence 3.4% (31)). Plots show reductions for Scenario 2 (2% rollout/day, realized $R = 1.5$) when vaccines are given to all individuals (solid lines) or to only seronegatives (dashed lines), inclusive of imperfect serotest sensitivity and specificity. Black dots indicate breakpoints at which prioritized demographic groups have been 70% vaccinated, after which vaccines are distributed without prioritization. Shown: contact patterns and demographics for the United States (22, 23); all-or-nothing and transmission-blocking vaccine with vaccine efficacy=90%. See Figs. 4 and S13 for moderate and higher seroprevalence examples, respectively.

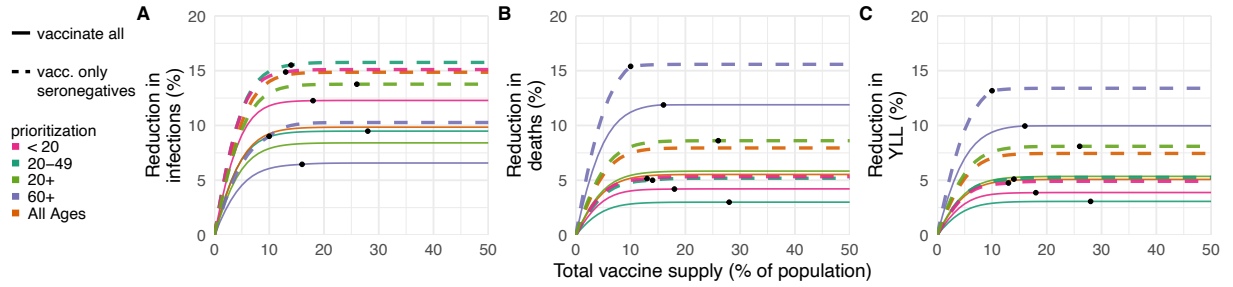


Figure S13: **Effects of existing seropositivity on the impacts of prioritization strategies (high seroprevalence).** Percent reductions in (A) infections, (B) deaths, and (C) years of life lost (YLL) for prioritization strategies when existing age-stratified seroprevalence is incorporated (model-generated; mean seroprevalence 40.1%; see Methods) and initial conditions are set to the S, E, I, and R compartment counts at the mid-outbreak time when seroprevalence reached 40.1%. Plots show reductions with 2% rollout/day, $R_0 = 2.6$, and realized $R = 1.43$ when vaccines are given to all individuals (solid lines) or to only seronegatives (dashed lines), inclusive of imperfect serotest sensitivity and specificity. Black dots indicate breakpoints at which prioritized demographic groups have been 70% vaccinated, after which vaccines are distributed without prioritization. Shown: U.S. contact patterns and demographics (22, 23); all-or-nothing and transmission-blocking vaccine with vaccine efficacy = 90%. See Figs. 4 and S12 for moderate and lower seroprevalence examples, respectively.

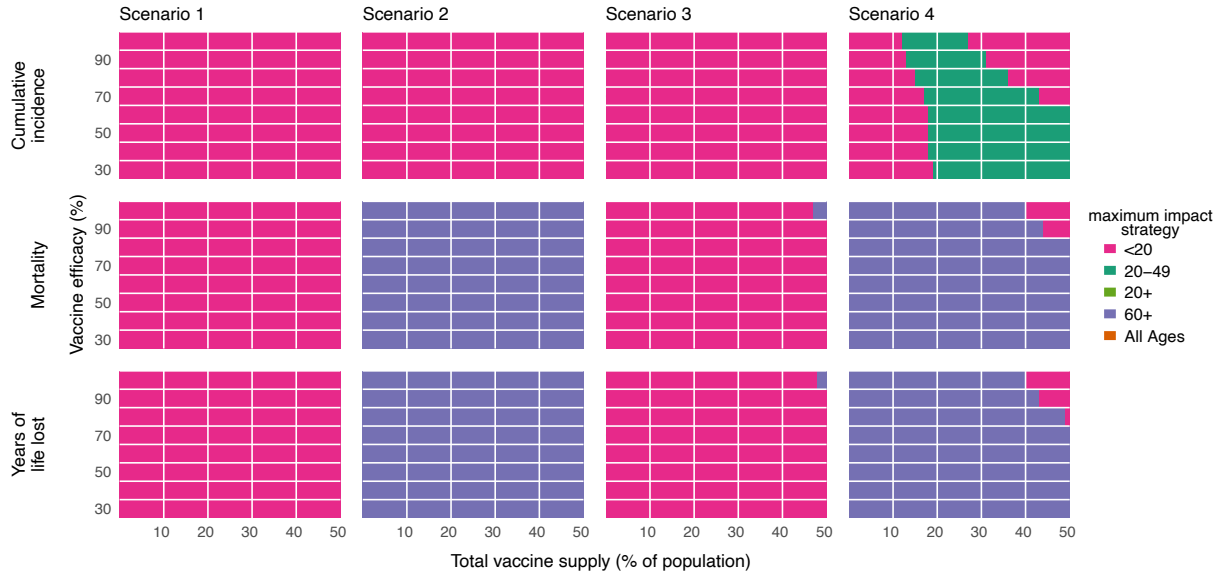


Figure S14: **Impact of vaccine efficacy on maximum impact strategies (all-or-nothing vaccine; constant susceptibility by age).** Heatmaps show the prioritization strategies resulting in maximum reduction of infections (top row), mortality (middle row), and years of life lost (bottom row) across Scenario 1 (0.2% rollout/day, $R_0 = 1.15$; left column), Scenario 2 (0.2% rollout/day, $R_0 = 1.5$; left-middle column), Scenario 3 (pre-transmission vaccination, $R_0 = 1.5$; right-middle column), and Scenario 4 (pre-transmission vaccination, $R_0 = 2.6$; right column). Each heatmap shows results from simulations varying vaccine supply and vaccine efficacy as indicated, but unlike all other simulations in this manuscript and its supplementary material, except Fig. S15, simulations use a constant susceptibility by age. Shown: contact patterns and demographics of the United States (22, 23); all-or nothing and transmission blocking vaccine. See Fig. S15 for leaky vaccine results with constant susceptibility by age. See Fig. S5 for all-or-nothing vaccine results with varying susceptibility by age.

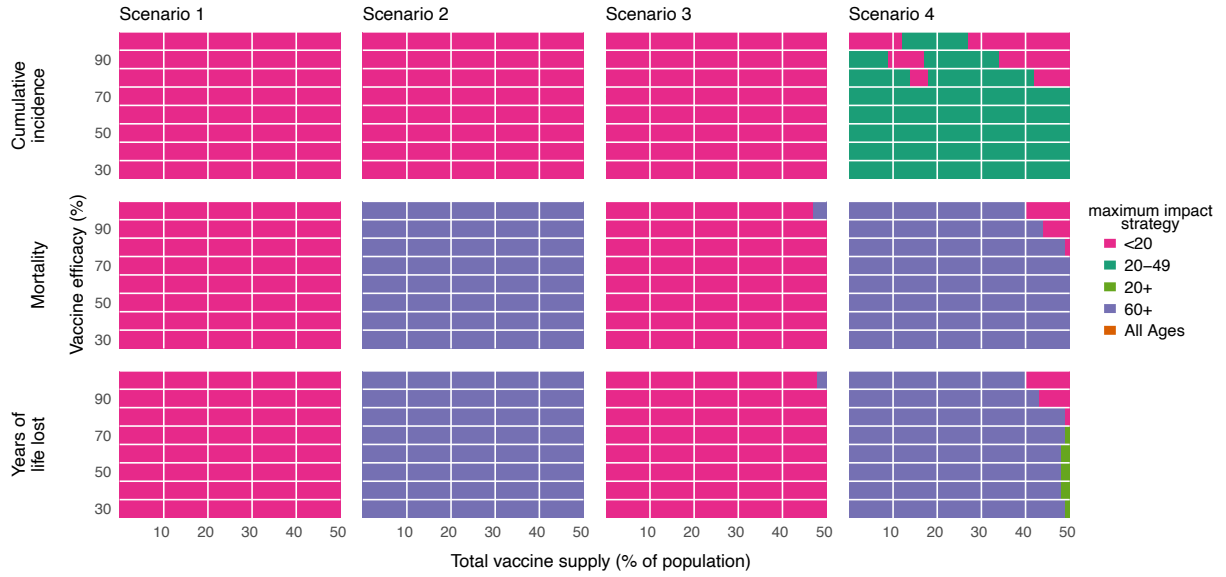


Figure S15: **Impact of vaccine efficacy on maximum impact strategies (leaky vaccine; constant susceptibility by age).** Heatmaps show the prioritization strategies resulting in maximum reduction of infections (top row), mortality (middle row), and years of life lost (bottom row) across Scenario 1 (0.2% rollout/day, $R_0 = 1.15$; left column), Scenario 2 (0.2% rollout/day, $R_0 = 1.5$; left-middle column), Scenario 3 (pre-transmission vaccination, $R_0 = 1.5$; right-middle column), and Scenario 4 (pre-transmission vaccination, $R_0 = 2.6$; right column). Each heatmap shows results from simulations varying vaccine supply and vaccine efficacy as indicated, but unlike all other simulations in this manuscript and its supplementary material, except Fig. S14, simulations use a constant susceptibility by age. Shown: contact patterns and demographics of the United States (22, 23); leaky and transmission blocking vaccine. See Fig. S14 for all-or-nothing vaccine results with constant susceptibility by age. See Fig. S7 for leaky vaccine results with varying susceptibility by age.

Supplementary Tables

Parameter	Description	Value	Reference
d_E	Latent period	3 days	(13)
d_I	Infectious period	5 days	(13)
u_i	Relative susceptibility to infection for age- i individuals	[0.4, 0.38, 0.79, 0.86, 0.8, 0.82, 0.88, 0.74, 0.74]	(13)
IFR	Infection fatality rate	[0.001, 0.003, 0.01, 0.04, 0.12, 0.40, 1.36, 4.55, 15.24]*	(19)
N_i	Number of people in age group i	country-specific demographic data	(23)
θ_i	Percent of seropositive age- i individuals	New York**: [32.0, 31.29, 24.9, 24.9, 26.4, 27.9, 25.75, 22.15, 20.7] Connecticut**: [3.9, 3.82, 3.1, 3.1, 3.1, 3.7, 3.2, 2.7, 2.7]	(30)
c_{ij}	Number of age- j individuals contacted by an age- i individual per day	Country-specific contact matrix (home, work, school and other)	(22)

Table S1: **Summary of parameters used in modeling and simulation.**

* To relate the IFR metaregression result from (19), $\log_{10}(\text{IFR}) = -3.27 + 0.0524 * \text{age}$ to age bins by decade, we computed $\text{IFR}_i = (\sum_j \text{IFR}_j)/10$ where j are the ages (in years) corresponding to bin i .

** To relate NYC (30) and Connecticut (31) seroprevalence estimates to age bins by decade, we computed $\theta_i = (\sum_j \theta_j)/10$ where j are the ages (in years) corresponding to bin i .

IC*	Pre-transmission rollout, all-or-nothing ve	Pre-transmission rollout, leaky ve	Continuous rollout
$I_i(0)$	1		$0.0025 N_i(1 - vh)$
$I_{x,i}(0)$	1		$0.0025 N_i(vh)$
$E_i(0)$	0		$0.0025 N_i(1 - vh)$
$E_{x,i}(0)$	0		$0.0025 N_i(vh)$
$R_i(0)$	$\theta_i N_i(1 - vh) - \alpha_i \theta_i N_i(1 - vh)$		$\theta_i N_i(1 - vh)$
$R_{v,i}(0)$	$\alpha_i \theta_i N_i(1 - vh)(1 - se)$		0
$R_{x,i}(0)$	$\theta_i N_i(vh) + \alpha_i \theta_i N_i(1 - vh)se$		$\theta_i N_i(vh)$
$S_i(0)$	$S(1 - vh) - \alpha_i S(1 - vh)$		$(N_i - 0.005N_i - \theta_i N_i)(1 - vh)$
$S_{v,i}(0)$	NA	$\alpha_i S(1 - vh)(sp)$	0 if leaky ve , else NA
$V_i(0)$	$\alpha_i S(1 - vh)ve(sp)$	NA	0 if all-or-nothing ve , else NA
$S_{x,i}(0)$	$S(vh) +$ $\alpha_i S(1 - vh)(1 - sp) -$ $\alpha_i S(1 - vh)(1 - ve)(sp)$	$S(vh) +$ $\alpha_i S(1 - vh)(1 - sp)$	$(N_i - 0.005N_i - \theta_i N_i)(vh)$

Table S2: **Initial conditions for simulations.** Scenario initial conditions (ICs) for age group i are reported for scenarios considered in this manuscript. NA, Not Applicable; se , sensitivity; sp , specificity; vh , vaccine hesitant fraction. $S = N_i - I_i(0) - I_{x,i}(0) - \theta_i N_i$. The proportion of each age group that is vaccine hesitant is denoted vh and not considered for vaccination. Vaccination rollout $\alpha_i = n_{\text{vax},i} / [(S_i + E_i)sp + R_i(1 - se)]$. Note that modeling without targeting of seronegatives via serological testing is equivalent to setting $sp = 1$ and $se = 0$.

* ICs for all other compartments not explicitly specified are 0.

References and Notes

1. COVID-19 Dashboard by the Center for Systems Science and Engineering at Johns Hopkins University, Online (2020); <https://coronavirus.jhu.edu/map.html>.
2. R. Khamsi, If a coronavirus vaccine arrives, can the world make enough? *Nature* **580**, 578–580 (2020). [doi:10.1038/d41586-020-01063-8](https://doi.org/10.1038/d41586-020-01063-8) [Medline](#)
3. Framework for equitable allocation of COVID-19 vaccine, Online (2020); www.nap.edu/catalog/25917/framework-for-equitable-allocation-of-covid-19-vaccine.
4. D. Weycker, J. Edelsberg, M. E. Halloran, I. M. Longini Jr., A. Nizam, V. Ciuryla, G. Oster, Population-wide benefits of routine vaccination of children against influenza. *Vaccine* **23**, 1284–1293 (2005). [doi:10.1016/j.vaccine.2004.08.044](https://doi.org/10.1016/j.vaccine.2004.08.044) [Medline](#)
5. J. Medlock, A. P. Galvani, Optimizing influenza vaccine distribution. *Science* **325**, 1705–1708 (2009). [doi:10.1126/science.1175570](https://doi.org/10.1126/science.1175570) [Medline](#)
6. S. Bansal, B. Pourbohloul, L. A. Meyers, A comparative analysis of influenza vaccination programs. *PLOS Med.* **3**, e387 (2006). [doi:10.1371/journal.pmed.0030387](https://doi.org/10.1371/journal.pmed.0030387) [Medline](#)
7. L. Matrajt, J. Eaton, T. Leung, E. R. Brown, *medRxiv* (2020). <https://www.medrxiv.org/content/10.1101/2020.08.14.20175257v3>.
8. M. E. Gallagher *et al.*, *medRxiv* (2020). <https://www.medrxiv.org/content/early/2020/08/11/2020.08.07.20170456>.
9. J. H. Buckner, G. Chowell, M. R. Springborn, *medRxiv* (2020). <https://www.medrxiv.org/content/10.1101/2020.09.22.20199174v4>.
10. F. Sandmann *et al.*, *medRxiv* (2020). <https://www.medrxiv.org/content/10.1101/2020.09.24.20200857v1>.
11. C. J. Worby, H.-H. Chang, Face mask use in the general population and optimal resource allocation during the COVID-19 pandemic. *Nat. Commun.* **11**, 4049 (2020). [doi:10.1038/s41467-020-17922-x](https://doi.org/10.1038/s41467-020-17922-x) [Medline](#)
12. E. Goldstein, M. Lipsitch, M. Cevik, On the effect of age on the transmission of SARS-CoV-2 in households, schools and the community. *J. Infect. Dis.* **2020**, jiaa691 (2020). [doi:10.1093/infdis/jiaa691](https://doi.org/10.1093/infdis/jiaa691) [Medline](#)
13. N. G. Davies, P. Klepac, Y. Liu, K. Prem, M. Jit, R. M. Eggo; CMMID COVID-19 working group, Age-dependent effects in the transmission and control of COVID-19 epidemics. *Nat. Med.* **26**, 1205–1211 (2020). [doi:10.1038/s41591-020-0962-9](https://doi.org/10.1038/s41591-020-0962-9) [Medline](#)
14. J. Zhang, M. Litvinova, Y. Liang, Y. Wang, W. Wang, S. Zhao, Q. Wu, S. Merler, C. Viboud, A. Vespignani, M. Ajelli, H. Yu, Changes in contact patterns shape the dynamics of the COVID-19 outbreak in China. *Science* **368**, 1481–1486 (2020). [doi:10.1126/science.abb8001](https://doi.org/10.1126/science.abb8001) [Medline](#)
15. S. Herzog *et al.*, *medRxiv* (2020). <https://www.medrxiv.org/content/10.1101/2020.06.08.20125179v3>.

16. A. L. Mueller, M. S. McNamara, D. A. Sinclair, Why does COVID-19 disproportionately affect older people? *Aging (Albany NY)* **12**, 9959–9981 (2020).
[doi:10.18632/aging.103344](https://doi.org/10.18632/aging.103344) [Medline](#)
17. Y. Liu, B. Mao, S. Liang, J.-W. Yang, H.-W. Lu, Y.-H. Chai, L. Wang, L. Zhang, Q.-H. Li, L. Zhao, Y. He, X.-L. Gu, X.-B. Ji, L. Li, Z.-J. Jie, Q. Li, X.-Y. Li, H.-Z. Lu, W.-H. Zhang, Y.-L. Song, J.-M. Qu, J.-F. Xu; Shanghai Clinical Treatment Experts Group for COVID-19, Association between age and clinical characteristics and outcomes of COVID-19. *Eur. Respir. J.* **55**, 2001112 (2020). [doi:10.1183/13993003.01112-2020](https://doi.org/10.1183/13993003.01112-2020)
[Medline](#)
18. J. Westmeier *et al.*, *mBio* **11**, e02243-20 (2020).
19. A. T. Levin, W. P. Hanage, N. Owusu-Boaitey, K. B. Cochran, S. P. Walsh, G. Meyerowitz-Katz, Assessing the age specificity of infection fatality rates for COVID-19: Systematic review, meta-analysis, and public policy implications. *Eur. J. Epidemiol.* **35**, 1123–1138 (2020). [doi:10.1007/s10654-020-00698-1](https://doi.org/10.1007/s10654-020-00698-1) [Medline](#)
20. H. Salje, C. Tran Kiem, N. Lefrancq, N. Courtejoie, P. Bosetti, J. Paireau, A. Andronico, N. Hozé, J. Richet, C.-L. Dubost, Y. Le Strat, J. Lessler, D. Levy-Bruhl, A. Fontanet, L. Opatowski, P.-Y. Boelle, S. Cauchemez, Estimating the burden of SARS-CoV-2 in France. *Science* **369**, 208–211 (2020). [doi:10.1126/science.abc3517](https://doi.org/10.1126/science.abc3517) [Medline](#)
21. J. K. H. Lee, G. K. L. Lam, T. Shin, J. Kim, A. Krishnan, D. P. Greenberg, A. Chit, Efficacy and effectiveness of high-dose versus standard-dose influenza vaccination for older adults: A systematic review and meta-analysis. *Expert Rev. Vaccines* **17**, 435–443 (2018).
[doi:10.1080/14760584.2018.1471989](https://doi.org/10.1080/14760584.2018.1471989) [Medline](#)
22. T. M. E. Govaert, C. T. Thijs, N. Masurel, M. J. Sprenger, G. J. Dinant, J. A. Knottnerus, The efficacy of influenza vaccination in elderly individuals. A randomized double-blind placebo-controlled trial. *JAMA* **272**, 1661–1665 (1994).
[doi:10.1001/jama.1994.03520210045030](https://doi.org/10.1001/jama.1994.03520210045030) [Medline](#)
23. J. A. Lewnard, S. Cobey, Immune History and Influenza Vaccine Effectiveness. *Vaccines (Basel)* **6**, 28 (2018). [doi:10.3390/vaccines6020028](https://doi.org/10.3390/vaccines6020028) [Medline](#)
24. S. F. Lumley *et al.*, *N. Engl. J. Med.* 10.1056/NEJMoa2034545 (2020).
25. City of New York, COVID-19 data, (2020); www1.nyc.gov/site/doh/covid/covid-19-data-testing.page.
26. K. L. Bajema *et al.*, *JAMA Intern. Med.* 10.1001/jamainternmed.2020.7976 (2020).
27. H. Ward *et al.*, *medRxiv* (2020).
<https://www.medrxiv.org/content/10.1101/2020.10.26.20219725v1>.
28. J. M. Dan *et al.*, *bioRxiv* (2020).
<https://www.biorxiv.org/content/10.1101/2020.11.15.383323v2>.
29. D. B. Larremore *et al.*, *medRxiv* (2020).
<https://www.medrxiv.org/content/10.1101/2020.04.15.20067066v2>.
30. D. Ellenberger, R. A. Otten, B. Li, M. Aidoo, I. V. Rodriguez, C. A. Sariol, M. Martinez, M. Monsour, L. Wyatt, M. G. Hudgens, E. Kraiselburd, B. Moss, H. Robinson, T. Folks, S.

- Butera, HIV-1 DNA/MVA vaccination reduces the per exposure probability of infection during repeated mucosal SHIV challenges. *Virology* **352**, 216–225 (2006). [doi:10.1016/j.virol.2006.04.005](https://doi.org/10.1016/j.virol.2006.04.005) [Medline](#)
31. K. E. Langwig, A. R. Wargo, D. R. Jones, J. R. Viss, B. J. Rutan, N. A. Egan, P. Sá-Guimarães, M. S. Kim, G. Kurath, M. G. M. Gomes, M. Lipsitch, Vaccine Effects on Heterogeneity in Susceptibility and Implications for Population Health Management. *mBio* **8**, e00796-17 (2017). [doi:10.1128/mBio.00796-17](https://doi.org/10.1128/mBio.00796-17) [Medline](#)
 32. H. R. Sharpe, C. Gilbride, E. Allen, S. Belij-Rammerstorfer, C. Bissett, K. Ewer, T. Lambe, The early landscape of coronavirus disease 2019 vaccine development in the UK and rest of the world. *Immunology* **160**, 223–232 (2020). [doi:10.1111/imm.13222](https://doi.org/10.1111/imm.13222) [Medline](#)
 33. M. Kornfield, *Washington Post* (2020). <https://www.washingtonpost.com/health/2020/12/02/kids-vaccine-delay/>.
 34. K. Prem *et al.*, *medRxiv* (2020). <https://www.medrxiv.org/content/10.1101/2020.07.22.20159772v2>.
 35. C. I. Jarvis, K. Van Zandvoort, A. Gimma, K. Prem, P. Klepac, G. J. Rubin, W. J. Edmunds; CMMID COVID-19 working group, Quantifying the impact of physical distance measures on the transmission of COVID-19 in the UK. *BMC Med.* **18**, 124 (2020). [doi:10.1186/s12916-020-01597-8](https://doi.org/10.1186/s12916-020-01597-8) [Medline](#)
 36. J. A. Backer *et al.*, *medRxiv* (2020). <https://www.medrxiv.org/content/10.1101/2020.05.18.20101501v2>.
 37. M. Brenan, Willingness to Get COVID-19 Vaccine Ticks Up to 63% in U.S., Online (December 8, 2020). <https://news.gallup.com/poll/327425/willingness-covid-vaccine-ticks.aspx>.
 38. S. Ghisolfi *et al.*, *Center for Global Development* (2020).
 39. M. Lipsitch, N. E. Dean, Understanding COVID-19 vaccine efficacy. *Science* **370**, 763–765 (2020). [doi:10.1126/science.abe5938](https://doi.org/10.1126/science.abe5938) [Medline](#)
 40. L. E. Duijzer, W. L. van Jaarsveld, J. Wallinga, R. Dekker, Dose-Optimal Vaccine Allocation over Multiple Populations. *Prod. Oper. Manag.* **27**, 143–159 (2018). [doi:10.1111/poms.12788](https://doi.org/10.1111/poms.12788) [Medline](#)
 41. T. Takahashi, M. K. Ellingson, P. Wong, B. Israelow, C. Lucas, J. Klein, J. Silva, T. Mao, J. E. Oh, M. Tokuyama, P. Lu, A. Venkataraman, A. Park, F. Liu, A. Meir, J. Sun, E. Y. Wang, A. Casanovas-Massana, A. L. Wyllie, C. B. F. Vogels, R. Earnest, S. Lapidus, I. M. Ott, A. J. Moore, A. Shaw, J. B. Fournier, C. D. Odio, S. Farhadian, C. Dela Cruz, N. D. Grubaugh, W. L. Schulz, A. M. Ring, A. I. Ko, S. B. Omer, A. Iwasaki; Yale IMPACT Research Team, Sex differences in immune responses that underlie COVID-19 disease outcomes. *Nature* **588**, 315–320 (2020). [doi:10.1038/s41586-020-2700-3](https://doi.org/10.1038/s41586-020-2700-3) [Medline](#)
 42. D. Chakravarty, S. S. Nair, N. Hammouda, P. Ratnani, Y. Gharib, V. Wagaskar, N. Mohamed, D. Lundon, Z. Dovey, N. Kyprianou, A. K. Tewari, Sex differences in SARS-CoV-2 infection rates and the potential link to prostate cancer. *Commun. Biol.* **3**, 374 (2020). [doi:10.1038/s42003-020-1088-9](https://doi.org/10.1038/s42003-020-1088-9) [Medline](#)

43. M. Webb Hooper, A. M. Nápoles, E. J. Pérez-Stable, COVID-19 and Racial/Ethnic Disparities. *JAMA* **323**, 2466–2467 (2020). [doi:10.1001/jama.2020.8598](https://doi.org/10.1001/jama.2020.8598) [Medline](#)
44. M. Jenco, *AAP News* (2020).
<https://www.aappublications.org/news/2020/08/27/covid19vaccinepriorities082620>.
45. J. Cohen, The line starts to form for a coronavirus vaccine. *Science* **369**, 15–16 (2020).
[doi:10.1126/science.369.6499.15](https://doi.org/10.1126/science.369.6499.15) [Medline](#)
46. S. Mishra, J. C. Kwong, A. K. Chan, S. D. Baral, Understanding heterogeneity to inform the public health response to COVID-19 in Canada. *CMAJ* **192**, E684–E685 (2020).
[doi:10.1503/cmaj.201112](https://doi.org/10.1503/cmaj.201112) [Medline](#)
47. L. Hawks, S. Woolhandler, D. McCormick, COVID-19 in Prisons and Jails in the United States. *JAMA Intern. Med.* **180**, 1041–1042 (2020).
[doi:10.1001/jamainternmed.2020.1856](https://doi.org/10.1001/jamainternmed.2020.1856) [Medline](#)
48. H. S. Badr *et al.*, *Lancet Infect. Dis.* 10.1016/S1473-3099(20)30861-6 (2020).
49. J. Ducharme, *Time* (2020); <https://time.com/5870041/COVID-19-neighborhood-risk>.
50. R Core Team, *R: A Language and Environment for Statistical Computing*, R Foundation for Statistical Computing, Vienna, Austria (2019).
51. K. E. Atkinson, *An Introduction to Numerical Analysis* (Wiley, New York, 1989), chap. 2, pp. 56–58, second edn.
52. P. A. Gross, A. W. Hermogenes, H. S. Sacks, J. Lau, R. A. Levandowski, The efficacy of influenza vaccine in elderly persons. A meta-analysis and review of the literature. *Ann. Intern. Med.* **123**, 518–527 (1995). [doi:10.7326/0003-4819-123-7-199510010-00008](https://doi.org/10.7326/0003-4819-123-7-199510010-00008)
[Medline](#)
53. P. Span, *New York Times* (2020). <https://www.nytimes.com/2020/06/19/health/vaccine-trials-elderly.html>.
54. K. M. Bubar *et al.*, COVID-19 vaccine prioritization code. Zenodo (2020).
[doi:10.5281/zenodo.4308794](https://doi.org/10.5281/zenodo.4308794).
55. W. G. H. Observatory, Life tables by country, (2016);
<https://apps.who.int/gho/data/view.main.LT62160?lang=en>.
56. U. N. D. of Economic, S. A. P. Division, World population prospects (2019);
<https://population.un.org/wpp>.
57. C. H. Geurtsvan Kessel *et al.*, *Nat. Commun.* **11**, 3436 (2020).